16th World Conference on Earthquake, 16WCEE 2017

Santiago Chile, January 9th to 13th 2017

Paper N° 819(Abstract ID)

Registration Code: S-S1461616889

Experimental Performance of Buckling Restrained Braces Subjected to Bidirectional Displacement Histories

X. Wei[(1)], M. Bruneau[(2)]

[(1)] *Graduate Research Assistant, Dept. of Civil, Structural, and Environmental Engineering, Uni. at Buffalo, Buffalo, NY 14260 (corresponding author). Email: xiaonewe@buffalo.edu*

[(2)] *Professor, Dept. of Civil, Structural, and Environmental Engineering, Uni. at Buffalo, Buffalo, NY 14260. Email: bruneau@buffalo.edu*

…

Abstract

Buckling Restrained Braces (BRBs) have been implemented in buildings and bridges on account of their stable and desirable hysteretic characteristics, ease of design and ability to limit seismically-induced structural damage and provide satisfactory seismic performance. The authors have proposed using BRB's across expansion joints in specially designed bidirectional bridge ductile diaphragms to resist bidirectional earthquake excitations. Such an implementation requires ensuring that the BRB can perform under large transverse displacement demands of the BRB's end connections. In this paper, quasi-static tests were performed on two types of BRBs (using a shake table to apply bi-directional displacement histories) to investigate their ultimate inelastic cyclic performance when subjected to bidirectional displacement protocols, created from demands induced by earthquakes. Two types of pin-connected BRBs were designed and tested: (1) BRB-1 with long end plates designed to bend laterally to accommodate the transverse displacement without developing instability; (2) BRB-2 with end plates designed to be connected to spherical bearings. The results showed that all the BRBs performed satisfactorily. They eventually failed after extensive cycles of inelastic deformation (due to local buckling and fracture of the yielding core, as typically the case for BRBs), but no end-plate experienced fracture or instability.

Keywords: Buckling Restrained Braces, Connections, Seismic Analysis, Bidirectional Displacement Demands

1. Introduction

Buckling Restrained Braces (BRBs), initially developed in Japan in the mid-1980s, have been studied and implemented with various materials and geometries in buildings and bridges all over the world. A BRB generally consists of a central core surrounded by a tube that restrains the core from axially buckling in compression. Since BRBs can prevent global buckling of the steel core by encasing it over its length, they have a superior resistance to low-cycle fatigue, being typically able to sustain a large significant number of hysteretic cycles at large ductility demands. BRBs can develop stable hysteresis when subjected to in-plane cyclic loading, provided the BRB's end connections are designed to ensure that BRBs can reach their design axial strength in the core plate without first having instability issues at their ends. The out-of-plane instability of the BRB has been observed in several BRBF tests (Aiken et al. [1]; Roeder et al.[2]; Tremblay et al.[3]; Tsai et al.[4]; Palmer et al.[5]).

Tsai et al.[4] reported the out-of-plane buckling of the gusset plate that connected a BRB to a column when a full-scale 3-story 3-bay BRBF reached 2% drift. Tsai and Hsiao [5] described the details of a gusset plate stiffened by adding edge stiffeners to improve the seismic performance of the BRBF, and suggested that the effective length factor, K, used to design the gusset plate, should be 0.65 and 2, for the cases with and without edge stiffeners, respectively. The AIJ [6] contains two models considered for preventing the global instability of bolted-end BRBs. The rationale for these two models is best explained by Koetaka et al.[7] and Takeuchi et al.[8], in which the stability of BRB per these two concepts were investigated, respectively. Differential equations for the compression member were formulated and the boundary conditions were used to obtain the buckling strength of the BRB/connection system, which consists of the connection and restrained zone. Palmer et al.[9] tested a full three-dimensional two-story frame, with one-bay BRBFs in each direction, having pin-ended BRBs. The BRBF were subjected to a bidirectional "cloverleaf" test protocols. Although the BRBs' core plates failed at 3.6% and 4.2% storey drifts, significant inelastic deformations and damage happened to the framing member of the system and the gusset plates. The ability of the BRBs in the BRBF to resist bidirectional loading relies on the bending flexibility of the gusset plates to which the BRBs were connected.

In this paper, BRBs' bidirectional displacement capacities are investigated as implemented in bidirectional ductile bridge diaphragms. New designs of BRB's end connections are proposed. Quasi-static tests were performed on two types of BRBs using the shake table to apply bidirectional displacement histories, to determine their ultimate inelastic cyclic performance and corresponding connection behaviors. Note that because BRBs in this implementation would span across the bridge expansion joints (for example, between the abutment and the bridge deck), the effect of thermal elongation and shortening of the bridge (which would impose axial displacement demands on the BRB) was also investigated by the authors, but is beyond the scope of this paper.

2. Bidirectional Ductile Diaphragm with BRBs

BRBs are studied to be implemented in the superstructure of a slab-on-girder steel bridge to improve its seismic performance, such as to create a bidirectional ductile End Diaphragm System (EDS) as shown in Fig. 1. The bridge has two pairs of structural fuses installed at each end of a span, in a configuration that coincides with the skew and longitudinal directions. BRBs are considered to be easily replaceable to provide ductile response to horizontal earthquake excitations acting from any direction.

A straight (nonskew) simply supported single-span steel slab-on-girder bridge is considered as the prototype bridge in this study. This bridge has girders spaced at 72" center-to-center. The height of the girder is 72". The deck is assumed to be supported on bidirectional sliding bearings or other bearings with neglibible strength to horizontal deformations at the abutment. The bridge length is assumed to be 100 ft. The weight of the bridge is 2000 kips. The corresponding benchmark simplified model is shown in Fig. 2, considering a rigid bridge deck as a floating span. The flexibility of the girder and slab is neglected, as well as the stiffness contribution from the bearing web stiffeners. To size the BRB specimens and assess the design displacements to consider in its testing, nonlinear time history analyses were performed for the nonskew benchmark bridge having the target BRB (circled in Fig. 2) as the longitudinal BRB of 100" in length and assumed yield strength of 40 kips. This longitudinal BRB, i.e. generic BRB, was assumed to have an inclination angle of 45 degree from the

bridge deck. The yield length ratio factor of the BRB was assumed to be 0.5. The material of the steel core was assumed to be A36 with expected yield strength of 42 ksi. The cross sectional area of the BRB steel core was designed as 0.95 in^2.

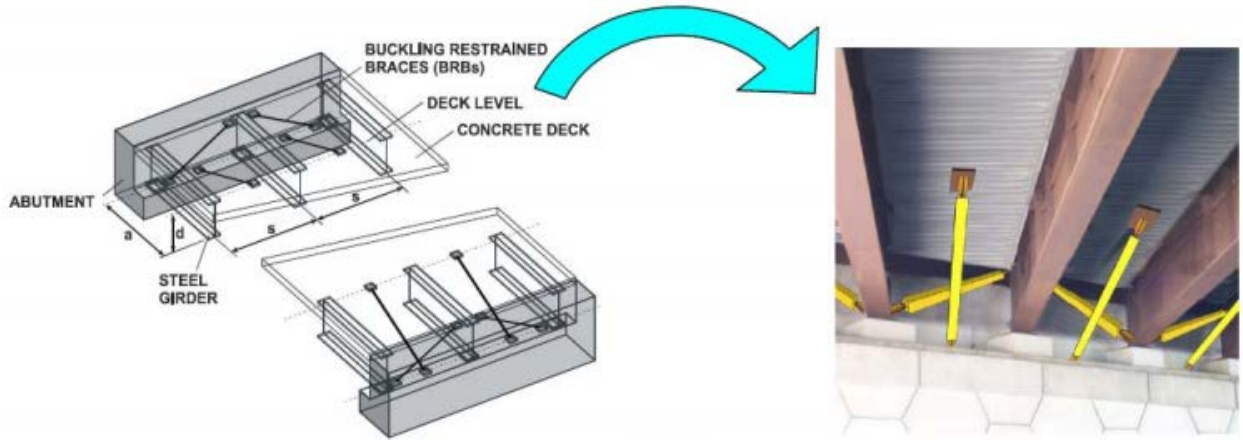

Fig. 1 – Bridge Ductile End Diaphragms with BRBs (Celik and Bruneau [10])

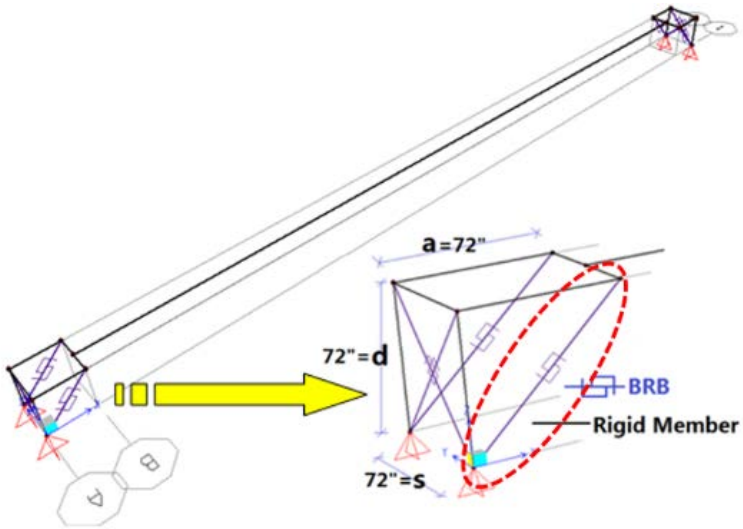

Fig. 2 –Bridge with BRBs in the EDS and enlarged view at the end

Orthogonal components of the ground motions records were inputted in the global longitudinal and transverse directions when performing the nonlinear time history analyses to investigate inelastic displacement demands of the BRB. The behaviors of the EDS in the two orthogonal directions are uncoupled and the system can be detailed to behave in the bilinear manner. The 44 ground motions specified in FEMA-P695 [11] were used to perform the nonlinear time history analyses of the benchmark bridge. The EDSs' displacement limits in both directions can translate into maximum global ductility demand, μ, themselves related to yielding displacement of the BRB in the EDS. The ground motions were scaled at each ductility level, and detailed information on scaling of the ground motions can be found in Wei and Bruneau [12].

Maximum transverse displacements of the bridge diaphragm model were obtained from 44 time history analyses using the 22 pairs of ground motions. Since the bidirectional displacement protocols were mainly intended to test the BRB's transverse displacement capacity, target ductilities up to 11 were considered in order to explore greater possible transverse displacement demands. The target ductility of 9 resulted in the largest transverse displacement of 1.602" among these ductility demands, with a corresponding longitudinal displacement demand of 0.913". The resulting average bidirectional displacement demand was 0.761" (same value in both directions), which was smaller than the global target displacement of 0.938" (corresponding to a

ductility of 9). The corresponding axial displacement demand of the BRB is 0.646", which was obtained by converting the longitudinal displacement demand considering the longitudinal BRB's inclination angle.

3. BRB Specimens and Test Setup

Two types of BRBs, namely BRB-1 and BRB-2, were designed and tested. They were manufactured and supplied by Star Seismic, LLC of Park City, Utah. Fig. 3 shows the side view of the typical BRB specimen with pin end connections. Both BRBs have two flat end plates with holes at their end, designed such that the BRB could be pin-connected to gusset plates in the reaction blocks located on the strong floor or the shake table, in the test setup shown in Fig.4. One end of the BRB was connected to a reaction block, itself tied down to holes in the strong floor. The other end was connected to the shake table, which was then used to apply horizontal end-displacement demands to the BRB. The BRB's core plate is encased in a concrete-filled steel hollow structural section (HSS). End Collars prevent instability of the core plate when it extends outside of the concrete restraining material.

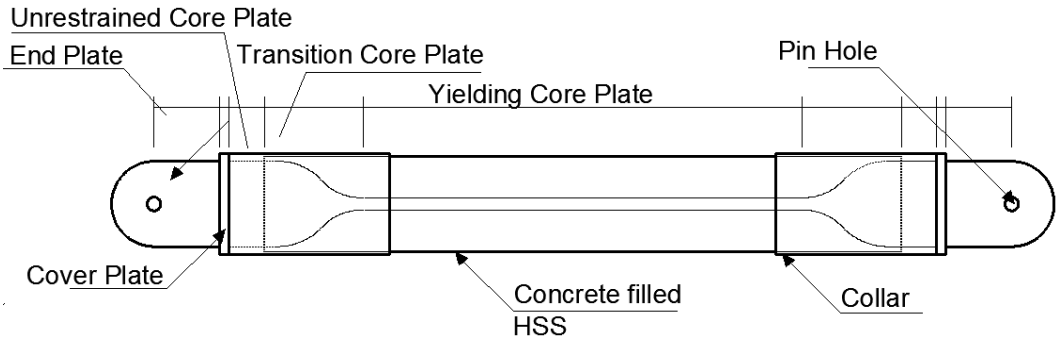

Fig. 3 –Side view of a typical BRB specimen

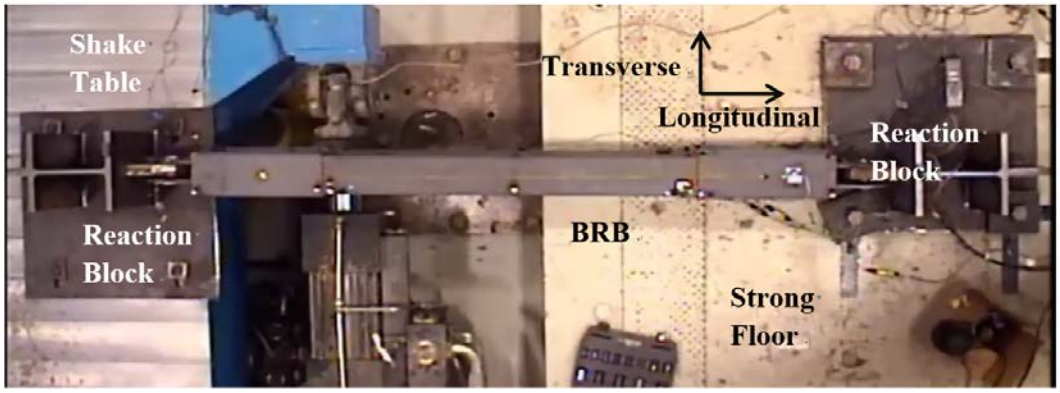

Fig. 4 –Quasi-static test setup with BRB

For the BRB with pin connections in the test layout shown in Fig. 4, each reaction block was made of a W-shape steel section, welded to a base plate, and gusset plates were welded to the W-shape and base plate. Note that because two different types of BRB were to be tested, two different types of gusset plates were needed to connect the BRBs to the reaction block. The reaction block gusset plates were designed to remain elastic when resisting the maximum tensile and compressive forces expected to be developed by the BRB, without yielding or buckling. Both gusset plates were made of A572Gr.50 steel. Gusset Plate-1 and Gusset Plate-2 were used to connect BRB-1 and BRB-2 as shown in Figs. 5 and 6, respectively. A bolt was used to connect the Gusset Plate-1 to BRB-1 at both ends. A spherical bearing allowing multi-directional movement was inserted to fit in the hole in the Gusset Plate-2 to connect to BRB-2 at both ends.

The BRBs' end connections need to sustain the required displacement demands when installed in the ductile bridge diaphragm, especially the transverse displacement that could cause the flexural yielding of the end plates of the BRB beyond the target design displacement. The end plates of BRB-1 were designed to bend laterally to accommodate the required lateral displacement without developing instability. The BRB's end plates

were sized such that the shake table's maximum displacement capacity could be used to test the BRB and examine the BRB's connection behavior beyond yielding and investigate its failure mode.

The end plates of BRB-2 were connected to a spherical bearing, itself kept in place in a pre-drilled hole in the gusset plates. Each spherical bearing works as a bi-directional hinge (similar to those that have been used by some dampers manufacturers). The maximum transverse displacement that BRB-2 can sustain depends on the design of the spherical bearing in the reaction block. It is recognized that special protection would be required when using spherical bearings in bridge applications, to prevent their corrosion.

The total pin-to-pin length of the BRB is 100 in, and their yield cores have a cross section area of 1.0 in^2. The material of the yielding steel core was specified as A36 with expected yield strength of 46 ksi. Other differences between BRB-1 and BRB-2 are listed:

• BRB-1 has a yielding core length of 46.5", while BRB-2's yielding core length is 50.2" (resulting in a yield length ratio of 0.46 and 0.5 for BRB-1 and BRB-2, respectively).

• The width of the unrestrained core plate part inside the BRB's collar is 5" and 9" for BRB-1 and BRB-2, respectively.

• The distance between the pin hole and the point where the end plates are connected to the cover plate is 11.5" and 5" for BRB-1 and BRB-2, respectively.

• The clear distance between the two end plates of BRB-1 is 1.25", and the pin hole size is 1 17/32". In comparison, the clear distance between the two end plates of BRB-2 is 2.5", and a 2" pin hole is used in which the spherical bearing is fitted.

Note that the actual BRBs have different properties than the generic BRBs used in the analyses of the benchmark bidirectional diaphragm model. The difference was considered in obtaining the test protocols presented later in this paper.

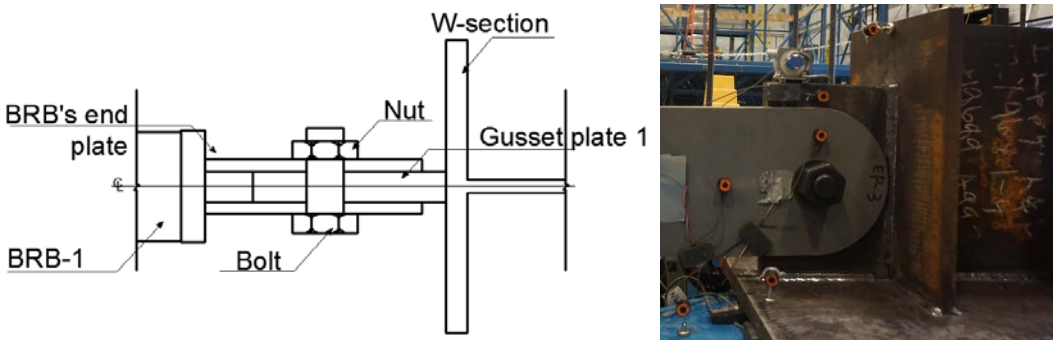

(a) (b)

Fig. 5 – (a) Section cut view of the details of BRB-1 with Gusset Plate-1 in the reaction block using the bolt connections; (b) Side-view photo of BRB-1 with reaction block connection in test setup

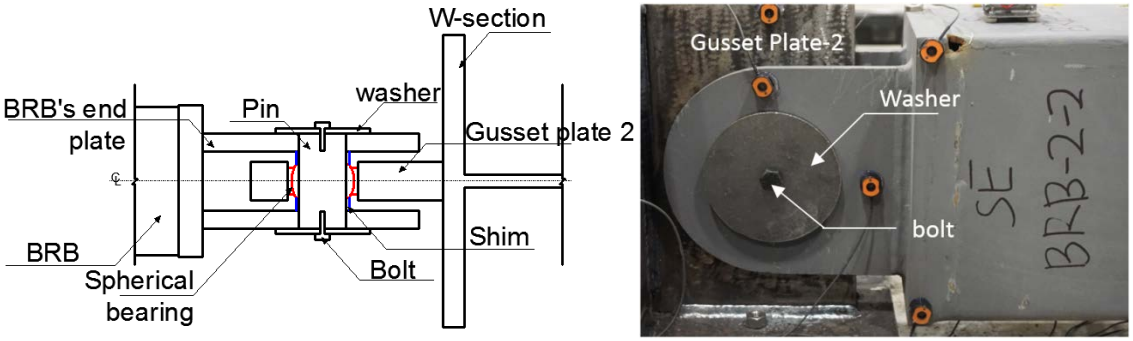

(a) (b)

Fig. 6 –(a) Section cut view of the details of BRB-2 with Gusset Plate-2 in the reaction block using the bolt connections; (b) Side-view photo of BRB-2 with reaction block connection in test setup

4. End Plate Design of BRB-1

For BRB-1, its transverse yield displacement, d_{yt} , is obtained when the end plate reaches its flexural yield strength at the bottom of the cantilevering end-plate under the BRB's maximum axial force. This transverse yield displacement should be larger than the target transverse displacement demand of 1.602", making sure that BRB's end connection would not yield in flexure. Fig. 7a shows the end plate of BRB-1 with a pin connection. The end plate has a clear length, L_{end} , from the bottom of the pin hole to its base. The width and thickness of the connecting end plate is *b* and *t*. The maximum force, *P*, considered applied through the pin connection is 90 kips, to account for strain hardening and material variability. The material for the end plates is assumed to be A36 with specified yield strength, f_{ye} , of 36 ksi.

The BRB end plates were designed as beam-columns with *K* of 2 to remain elastic under the maximum axial force that the BRB can develop, by avoiding yielding in tension and buckling in compression. Eq. D2-1 and D2-2 specified in AISC 360-10 [13] were used to calculate the plates' tensile strength. The compressive strength (buckling considered) was calculated based on Eq. E3-1, E3-2, E3-3 and E3-4 specified in AISC 360-10 [13]. The above equations were used to determine the maximum possible length of end plate, L_e, for which buckling in compression would be prevented for a given end plate cross section of $b \times t$, where *b* and *t* are the width and thickness of the end plate, respectively. The BRB's end plate was assumed to behave as a cantilever beam with cross section of $b \times t$ and length of L_e. For a lateral displacement applied to the BRB at its pin hole location, the cantilever beam would be under single curvature. The yield rotation of the end plate, θ_y, is obtained when the bottom of the end plate reaches its flexural yield strength. Considering that the BRB is also subjected to an axial force *P*, equal to the BRB's core yield force when maximum demands are reached in both directions, the flexural yield strength is reduced accordingly, and the yield curvature, φ_{ye} , when the expected yield stress, f_{ye}, is reached.

The transverse yield displacement of the BRB, d_{yt} , is calculated as the product of the end plate's end rotation, θ_y , and the total pin-to-pin length of the BRB, L_{brb} , as shown in Fig.7b. The largest transverse displacement demand over the end plate's flexural yield displacement ratio should be smaller than 1.0 to keep the BRB's end connection elastic in flexure. Thinner plates deflect more prior to yield and are more desirable in that perspective. However, this must be also balance by the fact that thinner plates are more prone to buckling.

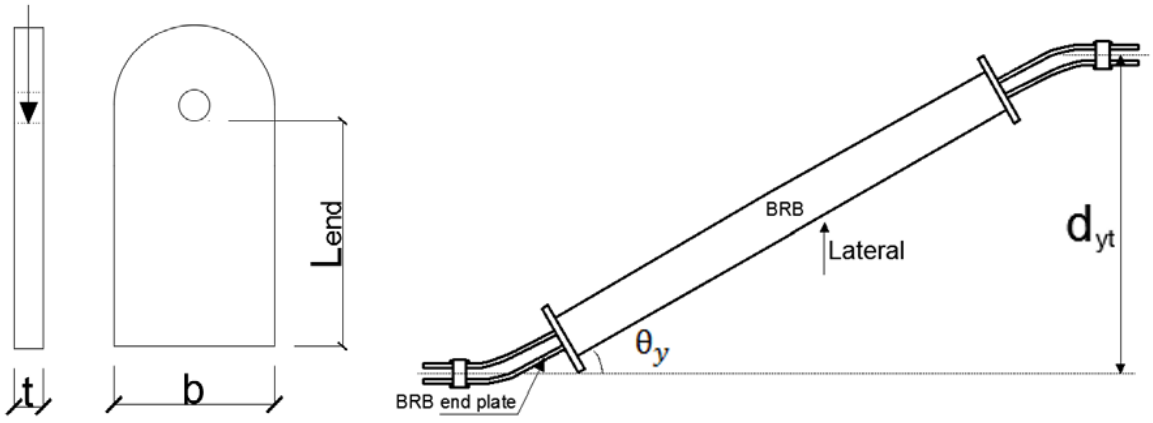

(a) (b)

Fig. 7- BRB-1: (a) end plate dimensions; (b) illustration of the relationship between BRB's transverse yield displacement vs the end plate yield rotation

To allow using a 1.5" diameter bolt to connect the BRB to the gusset plate, both Gusset plate-1 and the BRB-1 end plates had 1-17/32" holes. The end plate thickness, *t*, is 0.5", and the width of the end plates, *b*, is 9". The maximum total end plate length ratio of the BRB, $2L_e/L_{brb}$, is 0.217. For BRB-1 with a pin-to-pin length of 100", the corresponding maximum end plate's clear length, L_e , would be 10.85". For comparison, note that the BRB-1 specimen provided by Star Seismic had an end plate clear length of 10.75". The ratio of the largest transverse displacement of 1.602" over the end plate's flexural yield displacement is 0.83, confirming that the end plates would remain elastic at the maximum target transverse displacement demands.

5. Spherical Bearing Connection Design of BRB-2

The Gusset Plate-2 was designed to have a spherical bearing inserted into a hole in it as shown in Fig. 6a. A mounting pin (running through both the inner ring of the spherical bearing and the holes of the BRB plates) was used to connect the BRB to the Gusset Plate-2 of the reaction block. The bearing outer ring was tack welded by keeper rings to Gusset Plate-2 on both sides. Stainless steel shims, provided by the BRB manufacturers, were used on both sides of the spherical bearing to ensure that the gusset plate was centered in the clear space between the BRB's end plates. Two threaded holes were drilled at both ends of the pin, and a bolt and washer was used at each end to secure the pin within the BRB's end plates and prevent it from sliding out during cyclic loading.

The rotation capacity of the spherical bearing, γ, is 0.102 rad, obtained from the design manual for the specific type of spherical bearing used here. Furthermore, governing over the above limit in the current case, the maximum rotation that can be developed by the spherical bearing assembly is limited by the distance created between the BRB's end plates and the gusset plate by the bearing assembly geometry. In other words, the maximum rotation that can be developed is reached when the BRB's end plate becomes in contact with the gusset plate while the spherical bearing rotates; this rotation is labeled α_c as shown in Fig. 8. This value need not be greater than the rotation capacity of the spherical bearing itself. The calculated maximum rotation capacity α_c was 0.108 rad, which was larger than the spherical bearing's rotation limit γ of 0.102 rad for this case. Therefore, the bearing's rotation limit would be reached before the BRB's end plate touched the Gusset Plate-2. Note that, for the current pin-to-pin length of the BRB of 100", considering the displacement limits of the shake table of ±7" in both horizontal directions, the maximum possible rotational demand of the BRB in the transverse direction during the tests was limited to 0.07 rad. Therefore, for the planned tests using the shake table to apply BRB's transverse displacements, neither of the above rotation limits would be reached (i.e., the spherical bearing wouldn't reach their rotation limit and the gusset and end-plate would not come in contact). Also note that the spherical bearing design here only investigated strength and geometry requirements. Longevity issues related to materials between the sliding surface and the protection needed for the BRB to perform well in an exposed environment across bridges expansion joints still remain to be addressed. As expected, traverse displacements were not an issue for BRB having this spherical bearing connnection detail, and results are not included in this paper due to space constraints here. Complete results are available in Wei and Bruneau [12]

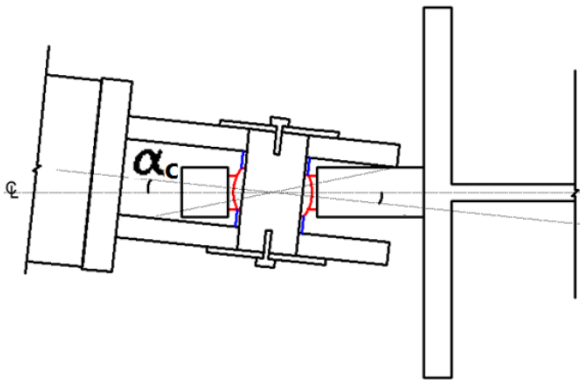

Fig. 8- Angles α_c related to the design of the spherical bearing in Gusset Plate-2

6. Instrumentation

A linear potentiometer (LP) was installed at each BRB end to measure the displacement between the collar and the HSS sleeve of the BRB. They were positioned at the top middle of the BRB as shown in Fig.9. The sum of the measured deformations from the two LPs is related to elongation of the BRB yielding core, assuming no rotation of the collars. The readings from those LPs, with accuracy on the order of 0.01", were expected to be more accurate than the SPs.

To capture the displacements of different parts in the BRB, the Krypton dynamic measurement machine was used, which has three sensitive infrared cameras mounted on a moveable frame, Light-Emitting Diodes (LEDs), and a data acquisition system. The LEDs are 1" in diameter and can be attached to any location visible

to the cameras. The three cameras would capture the locations of the LEDs in a user defined coordinate system. Accuracy of the krypton measurement is of the order of 0.004" and can be as high as 0.002", depending on the relative distance between the camera and the LEDs. The window of the Krypton camera in this test set-up was able to accommodate the entire BRB specimen and part of the reaction blocks on each end. Krypton camera was placed on the east side of the BRB specimen. It was used to capture the complete kinematics of the various parts of the BRB by recording the 3D movement of 32 LEDs attached to the BRBs and the reaction blocks. The layout of the LEDs used is shown in Fig. 10, with their numbering also marked out. The LEDs were all facing the negative-y direction (with respect to the Krypton coordinate system).

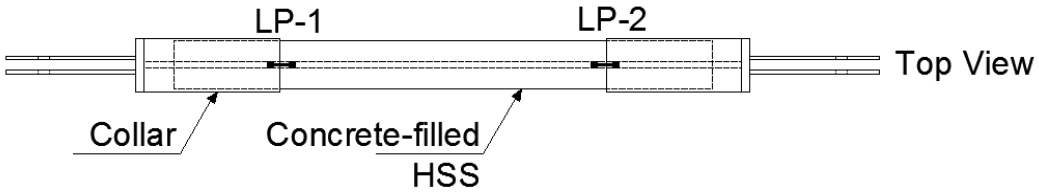

Fig. 9- Illustrations of locations of LPs in test specimens

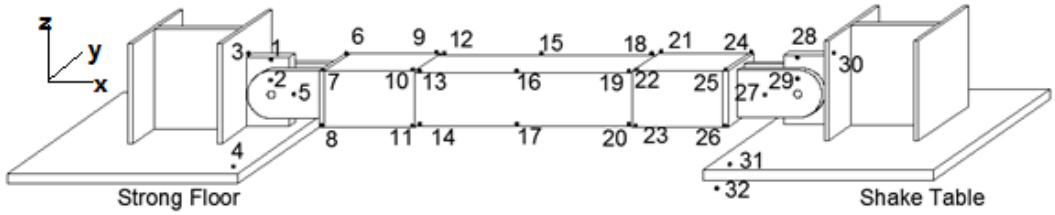

Fig. 10- Illustrations of LED locations in the test setup

The "BRB's axial deformation" is defined here, and calculated, based on the displacements between LED 2 and 29. In comparison, the "BRB's applied axial displacement" is defined here, and calculated, based on displacements between LED 1 and 28, which correspond to the sum of the "BRB's axial deformation" and the slippage of the pins (or bolts used as pins). Note that the terms BRB's axial deformation and BRB's applied axial displacement used throughout the text from here on refer to the above measures, which exclude and include slippage in the pins/bolts at the BRB ends, respectively. The other LEDs marked in Fig. 10 were used to obtain more informations regarding to the relative rotation between the collar and HSS, rotation and lateral displacement of the BRB end plates, slippage of the BRB pins in their holes, etc.. The BRB-1 specimens were also instrumented by stain gauges located on the end plates and the collar in an attempt to record their yielding. The detailed information of the strain gauges instrumented on the specimen is not presented here due to space constraints, which can be found in Wei and Bruneau [12].

7. Bi-directional Displacement Protocols

The standard test protocol used for the qualification test of BRBs is outlined in details in AISC 341-10 [14] and as follows: 2 cycles of loading at the deformations corresponding to $1.0D_{by}$, $0.5D_{bmL}$, $1.0D_{bmL}$, $1.5D_{bmL}$, $2.0D_{bmL}$, respectively followed by additional cycles of loading at the deformation corresponding to $1.5D_{bmL}$ as required for the specimen to achieve a cumulative inelastic axial deformation of at least 200 times the yield deformation. This protocol was developed for BRBs (tested alone and in sub-assemblies) principally subjected to axial displacements. Given that in the current proposed application in bi-directional diaphragms, BRBs are explicitly expected to be subjected to significant out-of-plane deformations in addition to axial ones, the existing test protocol had to be adapted.

The design objective for BRB-1 was that the BRB's end plates must not yield due to out-of-plane bending before the transverse displacement D_{bmT} is reached. Furthermore, AISC specifies that the BRB's core plate must sustain progressively increasing axial displacements until a value equal to twice the design displacement; it was therefore extrapolated here that it should also not fail at the twice the displacement demands in both directions during the bi-directional qualification test. Therefore, the bi-directional BRB test was conducted by controlling the level of axial (longitudinal) and transverse deformations imposed on the BRB, and by adapting the AISC requirements for the cyclic testing of BRBs. Bi-directionality was introduced in the test

protocol to investigate the BRB response by applying the biaxial S-type displacement pattern shown in Fig. 11. A complete large displacement loop is obtained by succession of the four small loops shown in Fig.11a, with movement of the shake table (looking from above) following the arrows. Each complete large loop in Fig. 11c was deemed equivalent to two of the cycles mentioned in the AISC test protocol because it imparted two full cycles of axial yield excursions. Therefore at each displacement step of the AISC protocol outlined above, only one complete bi-directional large loop was needed. Following the AISC protocol, the displacement demands for each large loop are increased incrementally after completing the previous cycle. The bi-directional qualification test protocol imposed displacements to the specimen until $2D_{bmL}$ and $2D_{bmT}$, were reached in both directions. A constant strain rate of 1.3×10^{-3} /s was used for this test protocol.

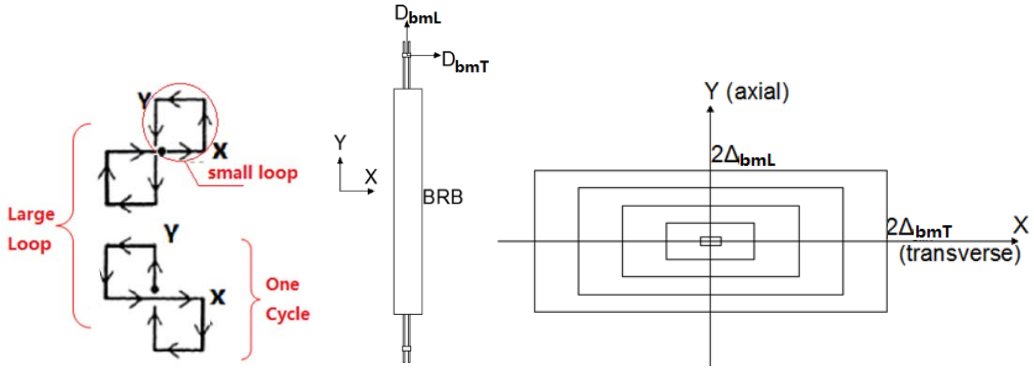

Fig.11-: Bi-axial s-type displacement pattern (a) small loops with arrows of movement; (b) BRB's longitudinal and transverse demand; (c) movement of one end of the BRB (connected to the shake table)

When obtaining the bi-directional displacement demands from the bridge with generic BRBs, the ground motion producing the largest displacement demands at the target ductility of 9 was selected as the "reference" motion. The decision of using the maximum displacement (resulting from all 22-pairs of ground motions) as the design target was revisited and found to be inconsistent with BRB design practice. This was because BRBs are typically designed for twice the design displacements, and design displacements are representative of average response, with the multiplier of 2 intended to account for maximum demands above the average. Therefore, it was decided to use the average displacement. This average displacement demand was obtained from new nonlinear time history analyses conducted with the actual BRB-1 properties and bridge characteristics. In these new analyses, the simplified bridge diaphragm model still had the same strength and stiffness in both the longitudinal and transverse direction. Besides, to limit the cumulative inelastic displacements reduced to approximately $200D_{by}$ at the end of the qualification test, the target design ductility was reduced to 6, which gave the design longitudinal and transverse displacement demand of 0.438"and 0.619", respectively. The corresponding cumulative inelastic displacement of the qualification test with these displacement demands is $208D_{by}$.

Due to bolt slippage, the elastic deformation and sliding of the reaction blocks, the BRB couldn't be directly subjected to the intended longitudinal displacement in the bidirectional displacement history, and adjustments were needed. The total displacement loss in the process of the BRB going from maximum tensile to maximum compressive force/displacement was estimated as 0.338" based on the test data from BRB-2. Half of that 0.338" displacement was added to the longitudinal displacement demand in each cycle of the bidirectional displacement history. The resulting bidirectional qualification displacement history with average displacement demand is shown in Fig.12.

In order to investigate the transverse displacement capacity of the BRB, the bidirectional test protocol in Fig.13 was also revised to have larger transverse displacements of 2", 4" and 6", while the longitudinal displacement demand remained at 1.5 times the design displacement, as shown in Fig. 13. The longitudinal displacement demand was kept at 1.5 times the design displacement, to be consistent with the standard BRB qualification test protocols described for additional cycles after the BRB has been subjected to the cycles at twice the design displacement. Note that, since the pin-to-pin length of the BRB is 100 in, the bidirectional

displacement histories at these three levels of transverse displacements correspond to drifts of 2%, 4% and 6%. They were labeled "BT2", "BT4", "BT6", respectively.

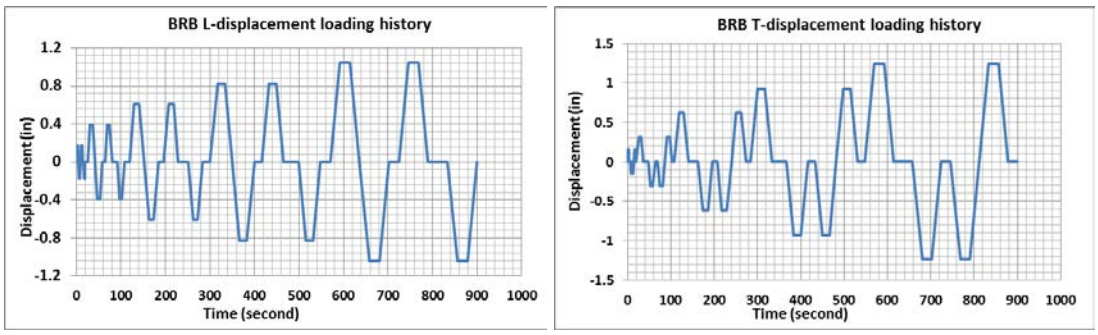

(a) (b)

Fig. 12- Average Bidirectional Qualification Displacement History for BRB-1 test: (a) longitudinal displacement vs time; (b) transverse displacement vs time; (c) loading sequence

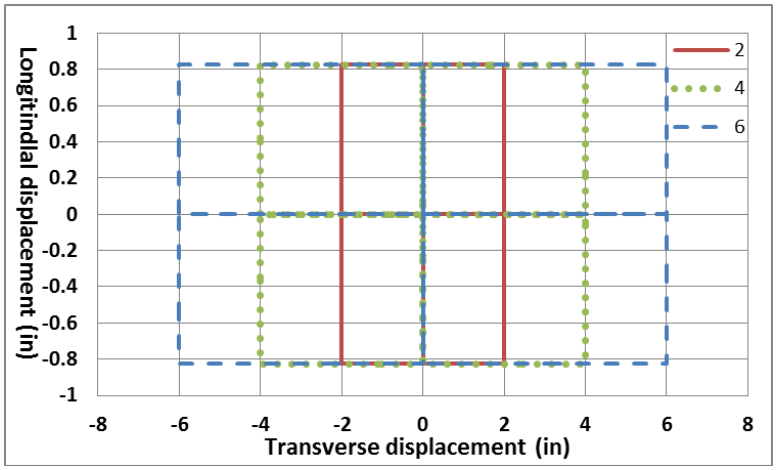

Fig. 13- Loops of Average Bidirectional Displacement History with increased transverse displacement demand: solid line (BT2), dotted line (BT4), dashed line (BT6)

8. Test of BRB-1

The bidirectional test protocol in Fig. 12 was applied to BRB-1 in test BRB-1-A. The specimen successfully passed the qualification test and the corresponding hysteretic curve of BRB-1's axial force versus axial deformation is shown in Fig. 14a. The BRB force versus applied axial displacements (in Fig. 14b) shows the bolt slippage at zero loads of 0.27". Stable inelastic behavior is observed.

In test BRB-1-B, BT2, BT4, BT6 were applied to the specimen sequentially, for one cycle each. The corresponding hysteretic behaviors of BRB-1 subjected to BT2, BT4, BT6 are shown in Figs 15a, 15b, 15c, with axial deformation measured by LPs and Krypton system in dotted and solid lines, respectively. The "indentation" of the hysteretic curves circles in Fig. 16 were caused by the BRB experiencing a small unloading and reloading when the table moved between the largest transverse displacements. This phenomenon became more apparent as the transverse displacement demand became larger. No end plate yielding occurred at 2% drift. At 4% and 6% drift, yielding happened close to the bolt hole on the west endplate, with a maximum recorded strain value of 2.06×10^{-3} and 4.41×10^{-3} in/in, respectively. Note that the maximum strain close to the east endplate bolt hole was 1.43×10^{-3} in/in (i.e., close to yielding).

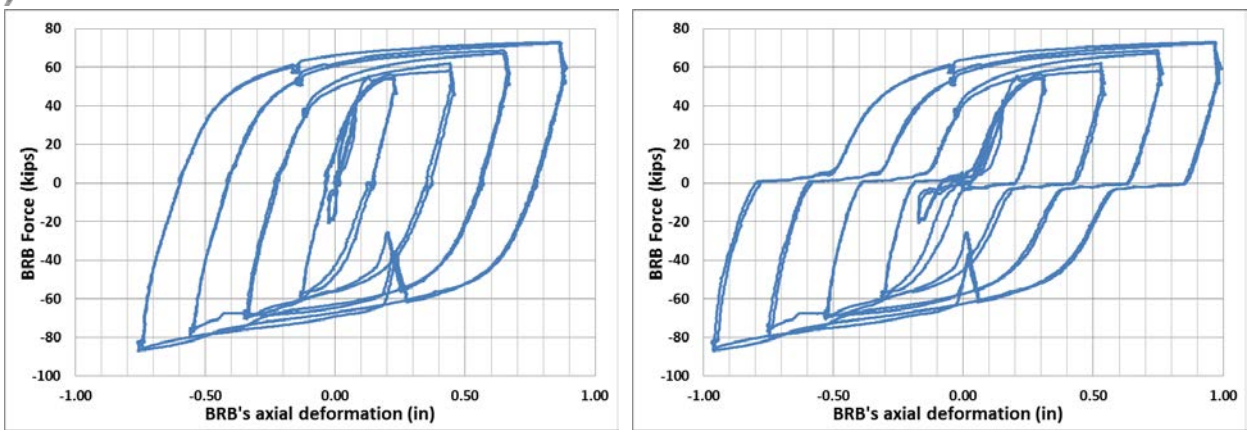

(a) (b)

Fig. 14- Hysteretic behavior of BRB-1 in test BRB-1-A: (a) axial force vs axial deformation; (b) axial force vs applied axial displacement

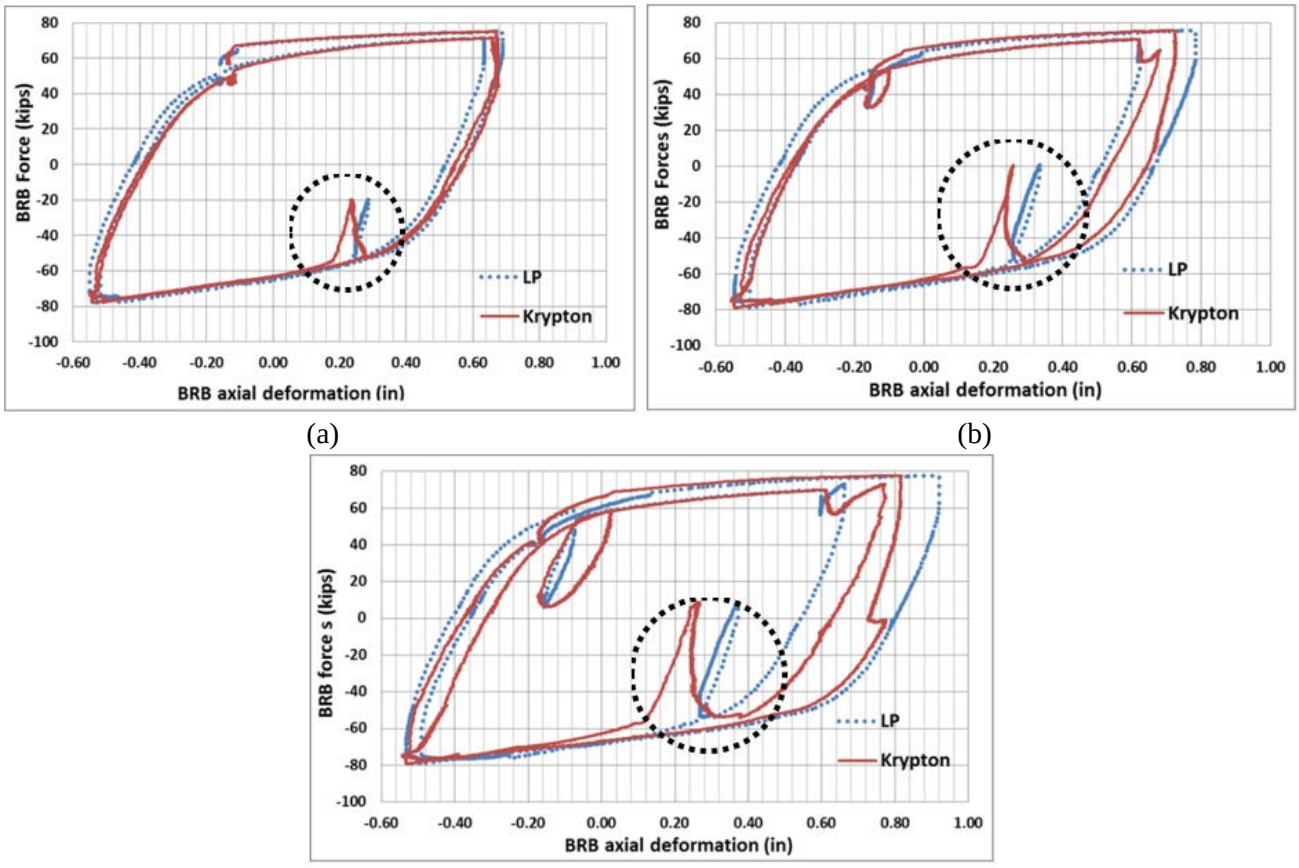

(a) (b)

(c)

Fig. 15- Hysteretic curves of BRB-1-3 subjected to (a) BT2, (b) BT4, and (c) BT6

To complete testing of the specimen already in place, BT6 was continuously applied to BRB-1 until the specimen failed during the 7th cycle at that magnitude of transverse displacement, in test BRB-1-C. Note that this is in addition to the BT6 applied to BRB-1 in test BRB-1-B. The hysteretic curves corresponding to the first four cycles of BT6 are identical to Fig. 15c, and therefore not shown here. The largest strain recorded by the strain gauges on the end plates in all the cycles of BT6 applied in BRB-1-C remained the same 4.41×10^{-3} in/in at the same location, which was close to the pin hole on the west end plate on the south side.

11. Conclusion

The BRB specimens with the specifically designed end connection details (either by having a long end plate or have the spherical bearing configuration) in the proposed bidirectional ductile diaphragm performed adequately, and sustained extensive cycles of inelastic deformations under bidirectional displacement test protocols. Both types of BRBs failed due to local buckling and fracture of the yielding core (typically the case for BRBs), and no end-plate experienced fracture or instability.

12. Acknowledgements

This research was funded by the Transportation Research Board of the National Academies under the TRB-IDEA Program (NCHRP-172). Special thanks is extended to Star Seismic for providing the BRB test specimens. The help and collective expertise from the staff of the Structural Engineering and Earthquake Simulation Laboratory at University at Buffalo are greatly appreciated.

13. References

[1] Aiken, I. D., Mahin, S. A., and Uriz, P. (2002). "Large-scale testing of buckling-restrained braced frames." *Proc., Japan Passive Control Symp.*, Tokyo Institute of Technology, Tokyo, 35e44.

[2] Roeder, C. W., Lehman, D. E., and Christopulos, A. (2006). "Seismic performance of special concentrically braced frames with buckling restrained braces." *Proc., 8th U.S. National Conf. on Earthquake Engineering*, Curran Associates, San Francisco

[3] Tremblay, R., Bolduc, P., Neville, R., and DeVall, R. (2006). "Seismic testing and performance of buckling-restrained bracing systems." *Can. J. Civ. Eng.*, 33(2), 183e198.

[4] Tsai, K. C, Hsiao, P. C., Wang, K. J., Weng, Y. T., Lin, M. L., Lin, K. C., Chen, C. H., Lai, J. W., and Lin, S. L. (2008). "Pseudo-Dynamic Tests of a Full-Scale CFT/BRB Frame-Part I: Specimen Design, Experiment and Analysis." *Earthquake Engineering & Structural Dynamics*, vol. 37, no. 7, 1081–1098.

[5] Palmer, K.,Roeder, C.,Lehman, D.,Okazaki, T., and Shield, C.(2013). "Experimental Performance of Steel Braced Frames Subjected to Bidirectional Loading." *J. Struct. Eng.*, 10.1061/(ASCE)ST.1943-541X.0000624, 1274-1284.

[6] Tsai, K. C., and Hsiao P. C. (2008). "Pseudo-Dynamic Test of a Full-Scale CFT/BRB Frame-Part II: Seismic Performance of Buckling Restrained Braces and Connections." *Earthquake Engineering & Structural Dynamics*, vol. 37, no. 7, 1099–1115.

[7] AIJ (2009): Architectural Institute of Japan: Recommendations for stability design of steel structures, Sec. 3.5 Buckling-Restrained Braces, 2009, 74–79.

[8] Koetaka Y, Kinoshita T, Inoue K, IItani K. (2008), "Criteria of buckling-restrained braces to prevent out-of-plane buckling", *Proceedings of 14th World Conference on Earthquake Engineering*, Beijing, China.

[9] Takeuchi, T., Ozaki, H., Matsui, R. and Sutcu, F. (2014), "Out-of-plane stability of buckling-restrained braces including moment transfer capacity." *Earthquake Engng Struct. Dyn.*, 43: 851–869. doi:10.1002/eqe.2376

[10] Celik, O., Bruneau, M., (2011). "Skewed Slab-on-Girder Steel Bridge Superstructures with Bidirectional-Ductile End Diaphragms," *ASCE Journal of Bridge Engineering*, Vol.16, No.2, pp.207-218.

[11] FEMA P-695, (2009): "Quantification of building seismic performance factors", prepared by Applied technology council for the federal emergency management agency, Washington DC

[12] Wei, X., Bruneau, M. (2016), "Buckling Restrained Braces Applications for Superstructure and Substructure Protection in Bridges", *Tech. Rep. MCEER-16-00xx*, MCEER, Uni. at Buffalo, Buffalo, NY

[13] AISC-360 (2010): "Specification for Structural Steel Buildings", American Institute of Steel Construction, Chicago, IL.

[14] AISC-341 (2010): "Seismic Provisions for Structural Steel Buildings", American Institute of Steel Construction, Chicago, IL.